On the effect of using collision/reaction cell (CRC) technology in single-particle ICP-mass spectrometry (SP-ICP-MS)

Eduardo Bolea-Fernandez[a], Diego Leite[b], Ana Rua-Ibarz[a,c], Tong Liu[a], Glenn Woods[d], Maite Aramendia[b,e], Martín Resano[b], Frank Vanhaecke[a*]

[a]Ghent University, Department of Chemistry, Atomic & Mass Spectrometry – A&MS research unit, Campus Sterre, Krijgslaan 281-S12, 9000 Ghent, Belgium

[b]University of Zaragoza, Aragón Institute of Engineering Research (I3A), Department of Analytical Chemistry, Pedro Cerbuna 12, 50009 Zaragoza, Spain

[c]Flemish Institute for Technological Research (VITO), Boeretang 200, 2400 Mol, Belgium

[d]Agilent Technologies LDA UK Ltd., 5500 Lakeside, Cheadle Royal Business Park, SK8 3GR Stockport, Cheshire, UK

[e]Centro Universitario de la Defensa de Zaragoza, Carretera de Huesca s/n, 50090 Zaragoza, Spain

[*]Corresponding author: Frank.Vanhaecke@UGent.be – Tel:+32(0)92644848 – Fax: +32(0)92644960

ABSTRACT

In this work, the effects of using collision/reaction cell (CRC) technology in quadrupole-based ICP-MS (ICP-QMS) instrumentation operated in single-particle (SP) mode have been assessed. The influence of (*i*) various CRC gases, (*ii*) gas flow rates, (*iii*) nanoparticle (NP) sizes and (*iv*) NP types was evaluated using Ag, Au and Pt NPs with both a traditional ICP-QMS instrument and a tandem ICP-mass spectrometer. It has been shown that using CRC technology brings about a significant increase in the NP signal peak width (from 0.5 up to 6 ms). This effect is more prominent for a heavier gas (*e.g.*, NH_3) than for a lighter one (*e.g.*, H_2 or He). At a higher gas flow rate and/or for larger particle sizes (>100 nm), the NP signal duration was prolonged to a larger extent. This effect of using CRC technology has

been further demonstrated by characterizing custom-made 50 and 200 nm Fe_3O_4 NPs (originally strongly affected by the occurrence of spectral overlap) using different CRC approaches (H_2 on-mass and NH_3 mass-shift). The use of NH_3 (monitoring of Fe as the $Fe(NH_3)_2^+$ reaction product ion at m/z = 90 amu) induces a significant peak broadening compared to that observed when using H_2 (6.10 ± 1.60 *vs.* 0.94 ± 0.49 ms). This extension of transit time can most likely be attributed to the collisions/interactions of the ion cloud generated by a single NP event with the CRC gas and it even precludes 50 nm Fe_3O_4 NPs to be detected when using the NH_3 mass-shift approach. Based on these results, the influence of a longer peak width on the accuracy of SP-ICP-MS measurement data (NP size, particle number density and mass concentration) must be taken into account when using CRC technology as a means to overcome spectral overlap. To mitigate the potential detrimental effect of using CRC technology in the characterization of NPs *via* SP-ICP-MS(/MS), the use of light gases and low gas flow rates is recommended.

Keywords: Nanoparticles, single-particle ICP-MS/(MS), collision/reaction cell, spectral overlap, chemical resolution, peak width

1. INTRODUCTION

Downscaling of materials to the size range of nanometers (≤ 100 nm in at least one dimension) can change their properties dramatically and lead to interesting new characteristics, which opens up new fields of application. Nowadays, such engineered nanoparticles (ENPs) are widely used in various fields, ranging from material manufacturing over environmental and life sciences to food processing.**[1, 2]** However, this massive use of ENPs is raising concern about their potential effects on the environment and human health,**[3, 4]** thus requiring the development of powerful and versatile analytical tools aiming at unraveling their behavior in, *e.g.*, environmental and biological processes.**[5]**

Inductively coupled plasma – mass spectrometry (ICP-MS) plays an important role in this context, as it can be deployed as a single-particle analyzer; this approach is called single-particle (SP) ICP-MS (SP-ICP-MS).**[6-10]** The theory of SP-ICP-MS for the characterization of colloids in aqueous suspensions was first described by Degueldre *et*. *al*.**[11]** Since then, the number of papers reporting on the use of SP-ICP-MS has grown exponentially.**[12, 13]** SP-ICP-MS is based on the one-by-one introduction of NPs into the ICP, in which they are individually vaporized, atomized and the atoms thus obtained ionized. The ion cloud thus formed is then introduced into the mass analyzer and the transmitted ions are finally detected. The signals thus produced are of extremely short duration (~0.5 ms) for conventional ICP-MS.**[14-17]** The number of signal "spikes" detected and their integrated intensity can be used to calculate the size distribution, particle number density and mass concentration.

Despite its potential, ICP-MS, and hence SP-ICP-MS, also suffers from drawbacks, the occurrence of spectral interferences being a major one.**[18-20]** Over the years, different strategies have been used to overcome spectral overlap, caused by atomic and/or polyatomic ions occurring at the same nominal mass-to-charge (m/z) ratio as that of the target nuclide. The use of high mass resolution in sector field ICP-MS (HR-SF-ICP-MS) instrumentation is an elegant approach to get rid of spectral interferences,**[21, 22]** but so far, this type of instrumentation has not been widely / routinely used

for single-particle analysis.**[23]** The development of (*i*) new HR-SF-ICP-MS instrumentation capable of performing ultra-fast measurements (at dwell times down to 10 µs),**[24, 25]** and of (*ii*) SP data treatment software (*e.g.*, Nanocount) and/or calculation tools (RIKILT Wageningen UR) might promote the use of HR-SF-ICP-MS in the context of NP characterization.**[23, 26, 27]** Alternatively, also the use of collision/reaction cell (CRC) technology in quadrupole-based ICP-MS (ICP-CRC-QMS) instrumentation is a versatile approach to overcome spectral interference and it has become even more attractive with the introduction of tandem ICP-mass spectrometry (ICP-MS/MS) in 2012.**[28-34]** ICP-MS/MS benefits from a better control over the ion-molecule processes occurring within the CRC, as a result of the double mass selection provided by the additional quadrupole located before the CRC. In addition, present-day ICP-QMS instruments are equipped with user-friendly software for SP data treatment, making this technique suited for straightforward NP characterization in routine applications.

However, the use of the CRC technology for overcoming spectral overlap also brings about specific challenges when aiming at operating ICP-CRC-QMS instrumentation in SP mode. So far, this topic has been scarcely studied. Kálomista *et al.***[19]** have recently demonstrated that pressurizing a CRC with an inert gas (for getting rid of spectral overlap relying on kinetic energy discrimination – KED) influences the signal duration of a single NP event. However, to the best of the authors' knowledge, no work to date has studied the potential effect of introducing reaction gases to avoid spectral overlap *via* chemical resolution, although this approach is widely used within the ICP-MS(/MS) community to achieve interference-free conditions for elemental analysis. Peak broadening and peak shape have been extensively studied in the case of hyphenation of, *e.g.*, chromatographic techniques or laser ablation (LA) as a sample introduction system to ICP-MS. Detection capabilities can be strongly degraded when working with wide chromatographic peaks,**[35]** while in the context of LA-ICP-MS, recent efforts have been devoted to minimize aerosol dispersion aiming to achieve shorter washout times, thus providing a better imaging resolution.**[36]** However, peak shape and duration have not been systematically addressed in the case of SP-ICP-MS yet, especially when using CRC

technology as a means to avoid spectral overlap. This can most likely be attributed to the fact that the shortest dwell times attainable with previous-generation ICP-MS instrumentations did not allow well-defined peaks to be obtained (unless the detection system was adapted in-house, e.g., by using a digital oscilloscope **[15]**), as these dwell times were usually longer than the duration of a single NP event. In other words, only recent ICP-MS instrumentation provides sufficient temporal resolution to accurately define the peak generated by a single NP event with multiple data points, instead of reporting a single data point per NP.**[17, 37-41]** Furthermore, when using shorter dwell times (≤0.1 ms) in SP-ICP-MS, a suitable data treatment software is required for the integration of the individual signal values composing the transient signal for every NP.

In this work, we aim at assessing the effects of pressurizing the CRC of two different ICP-QMS instruments (a single quadrupole and a tandem ICP-MS unit) operated in SP mode on the characterization of different NP types using different CRC gases. The conclusions derived from the use of Au, Ag and Pt model NPs were further tested by analyzing Fe_3O_4 NPs, which strongly suffer from the occurrence of spectral interference. From all results obtained, critical considerations on and practical recommendations for the use of CRC technology in ICP-MS operated in SP mode are provided.

2. EXPERIMENTAL

2.1. Standards, samples and reagents

Ultra-pure water was obtained from a Direct-Q Milli-Q system (Millipore, France). Ag, Au, Fe and Pt solutions prepared from commercially available 1 g L^{-1} single-element standards (Instrument Solutions, The Netherlands) were used for method development and calibration purposes. Various suspensions of spherical (nano)particles (nanoComposix Inc, Czech Republic) with different sizes and chemical compositions were used in this work: 50 (51 ± 6), 80 (79 ± 7), 100 (98 ± 13) and 200 (202 ± 29.7) nm Ag, 50 (49.9 ± 2.2, Ultra Uniform^{TM}), 70 (71 ± 9) and 100 (97 ± 10) nm Au, 50 (46.2 ± 5.1) and

70 (72.2 ± 4.2) nm Pt, and custom-made 50 (54 ± 5) and 200 (196 ± 64) nm Fe_3O_4. It needs to be noted that manufacturing monodisperse 200 nm Fe_3O_4 NPs proved difficult, resulting in a wider, bimodal size distribution (see section 3.2.). Size distributions, particle number densities and mass concentrations for these (nano)particle suspensions were provided by the manufacturer (determined by TEM and gravimetric analysis). Also, 75 nm AgNPs (74.6 ± 3.8, NIST SRM 8017) and 30 nm AuNPs (27.6 ± 2.3, NIST SRM 8012) from the National Institute of Standards Technology (NIST, USA) were used as NP reference materials for the determination of the transport efficiency (TE). Additionally, we also studied some of the NPs using TEM (Tecnai T20, ThermoFisher Scientific, USA) to validate the SP-ICP-MS measurements and/or to provide additional information for data interpretation. The NP suspensions were gently stirred and sonicated before appropriate dilution. For all the experiments intended to measure the average signal duration of individual NP events, no more than 3 000 NP events per minute were detected (generally, this value was lower than 1 000 NP events per minute). For the determination of the size distribution of FeNPs (see section 3.2.), dilution factors leading to less than 1 000 NPs per minute were used in all cases. It needs to be noted that all measurements were carried out at ultra-fast data acquisition speed (dwell time of 100 µs). The dilution factors were calculated based on Poisson statistics to minimize the occurrence of double events during SP-ICP-MS/(MS) measurement (see section 3.3.).

2.2. Instrumentation

All measurements were carried out using either of two quadrupole-based ICP-MS instruments: a NexION 300X (Perkin Elmer, USA) ICP-QMS instrument and an Agilent 8900 (Agilent Technologies, Japan) tandem ICP-MS/MS instrument. The NexION 300 is equipped with a quadrupole-based CRC (also known as dynamic reaction cell – DRC) and with a quadrupole ion deflector to bend the ion beam over a 90 degrees angle before its introduction into the CRC. Both the hardware and software of this instrument were upgraded to enable faster data adquisition (down to 1 value every 10 µs). The sample introduction system comprised a 0.5 mL min^{-1} concentric quartz nebulizer and a quartz cyclonic spray chamber. The Agilent 8900 is equipped with two quadrupole mass filters (Q1 and Q2)

and an octopole CRC cell mounted in-between. Use of the MS/MS mode facilitates the study of the reactions occurring within the CRC as a result of the different scanning tools available, such as precursor and product ion scans.**[34]**

In this work, the CRC of both instruments was pressurized with different gases, He, H_2 and NH_3/He (10% NH_3 in He), and the results thus obtained were compared with the standard "no gas" or "vented" mode. In addition, different on-mass and mass-shift approaches typically used for overcoming spectral overlap in ICP-CRC-QMS instrumentation were evaluated.

2.3. Data treatment

In addition to the SP software available in the MassHunter 4.4 Workstation for the Agilent 8900 ICP-MS/MS unit (Agilent Technologies, Inc. 2017) and the Nano Application module of the Syngistix software, version 2.1. for the NexION 300 X (Perkin Elmer Inc., 2018), an in-house developed Hyper Dimensional Image Processing (HDIP) software was used to accurately calculate the NP signal duration. This software was developed for post-processing of spectral data and images in the context of laser ablation (LA) ICP-MS and is meanwhile commercially available from Teledyne Cetac Technologies for this purpose, but was adapted to identify the individual NP events appearing randomly during SP-ICP-MS measurements. By using the HDIP software, the average signal duration (at different %-ages of the peak height) and the average peak shape of NP events measured under different conditions could be calculated easily (**Figure 1**). To prevent data calculation artefacts, such as a contribution from the background signal to the peak width, the selection criteria can be modified by adjusting the software settings. HDIP uses a peak-finding approach based on a parameter 'delta'. A data point is considered a "local maximum" when its intensity is higher than both that of the preceding and that of the subsequent data point by a value lower than delta times that maximum signal intensity. By using the delta parameter, the sensitivity of the peak detection algorithm can be adapted. This list of established maxima is further filtered by comparison of the corresponding intensities to a thresholding criterion: maxima below a cut-off value (a percentage of

the total signal height range) are rejected. Based on a sufficient number of peaks, peak statistics can be obtained and, when the algorithm is complete, the cumulative distribution function and average peak profile are shown. Off-line, outliers resulting from instrument-derived signal spikes or other artifacts resulting from the software data treatment were removed. For this purpose, any data point more than 1.5 interquartile ranges (IQRs) below the first quartile or above the third quartile was considered as an outlier.

3. RESULTS AND DISCUSSION

3.1. Effect of the CRC conditions on the signal duration of single NP events

3.1.1. Effect of CRC mode

To assess the effect of the CRC mode on the signal duration of single NP events, different methods were developed by pressurizing the CRC system of an ICP-MS/MS instrument with He, H_2 or NH_3 and by comparing the results thus obtained with those obtained in "no gas" or "vented" mode. These different methods were selected aiming to assess the potential influence of different strategies that are widely applied in ICP-QMS to overcome spectral overlap. An inert gas, such as He, can be used in the CRC to slow down polyatomic ions more than the atomic target ions, such that the former can be selectively removed *via* kinetic energy discrimination (KED mode), while in the case of H_2 and NH_3, a combination of collisions and reactions is relied on to overcome spectral overlap.**[28, 29, 32]** For this experiment, different methods for the detection of AuNPs were developed using an ICP-MS/MS instrument equipped with an octopole CRC, as this can be seen as the more suitable technique to study the in-cell chemistry in ICP-QMS.**[34]** In the case of no gas, He (5.0 mL min^{-1}) and H_2 (7.0 mL min^{-1}), Au^+ was monitored at its original mass-to-charge (m/z = 197 amu) ratio (on-mass), while with NH_3 (2.3 mL min^{-1} of a mixture of 10% NH_3 in He and an additional flow of 1 mL min^{-1} of He), both Au^+ and the best suited product ion of the reaction between Au^+ and NH_3 (mass-shift approach) were monitored. For mass-shift method development, the reactivity between Au^+ and NH_3 was assessed

using product ion scanning (PIS) at different NH_3 gas flow rates, and $Au(NH_3)^+$ (m/z = 214 amu) was identified as best suited reaction product ion. Instrument settings, including the axial acceleration (AA) function available for the Agilent 8900 ICP-MS/MS instrument (see section 3.2.1.), were optimized to achieve the highest signal-to-background ratio. It needs to be noted that the use of collision and/or reaction gases is (typically) not required for interference-free determination of Au,**[42]** and that the purpose of developing these methods was to evaluate the influence of various CRC modes on the characterization of NPs *via* SP-ICP-MS. It can be reasonably hypothesized that the most important conclusions drawn by studying AuNPs as "model NPs" can also be extrapolated to other NP types.

Table 1 and **Figure 2** show the effect of the different CRC modes on the signal duration and peak shape of individual NP events. For this experiment, highly monodisperse 50 nm AuNPs were measured using all modes, except for the NH_3 mass-shift approach, for which 100 nm AuNPs were selected due to the relatively low sensitivity of this method. To assess the potential influence of NP size on the signal duration, 100 nm AuNPs were also measured in "no gas" or "vented" mode, as a correlation between transit time of the ion cloud and particle diameter has earlier been reported on in literature.**[43]** This behaviour has been related with the lower kinetic energy of larger particles, thus traveling slower through the plasma and, thus, experiencing more diffusion and widening of the ion cloud.**[44]** However, under the experimental conditions of this study, no significant difference was found between 50 and 100 nm AuNPs (average peak width at 1% of the maximum height of 0.60 ± 0.10 and 0.61 ± 0.13 ms, respectively), suggesting that within this NP size range and in the case of "no gas" mode, the influence of NP size can be considered negligible compared to the effect caused by using the CRC technology. As can be seen, also no significant difference was found between the "no gas" and H_2 modes (0.63 ± 0.10 ms), while a slight increase in signal duration (0.74 ± 0.13 ms) was already noticed when pressurizing the CRC with He. However, this effect turned out to be drastically different when using NH_3, both for the on-mass and the mass-shift NH_3 methods, with a significant peak tailing leading to average peak widths at 1% of the maximum height of 2.59 ± 0.91

and 1.84 ± 0.86 ms for on-mass and mass-shift, respectively. This peak tailing of the ion burst and the specific peak shape of an individual NP event have been observed in previous works and have been related with the expansion of the ion cloud during the extraction through the sampler cone.**[16, 45]** However, based on the results obtained in this work, this effect is significantly increased by the use of CRC technology. In addition, **Table 1** and **Figure 2** also show an important peak broadening at 10 and 50% of the maximum height for both NH_3 methods, thus indicating that the effect of using NH_3 in the CRC is not merely limited to a longer peak tail.

These results demonstrated that the use of NH_3 gas into the CRC of an ICP-QMS instrument can strongly modify the occurrence of NP events during SP-ICP-MS analysis. The significant differences between the use of NH_3 and the other CRC gases can most likely be attributed to the larger size of NH_3 molecules compared to that of H_2 molecules and/or He atoms *i.e.*, the larger collisional cross-section of the CRC gas increases the probability of collision/interaction with the ion plume created for each NP event, thus significantly disturbing the kinetic energy distribution of the ions generated from a single NP. Consequently, some of those ions might lose kinetic energy to a different extent, and thus, they will be detected at slightly different moments in time (**Figure 3** illustrates the effect of pressurizing a CRC system during the measurement of the fast transient signal for an individual NP). This effect explains the longer peak width and the relatively long tail observed for the AuNPs measured using both NH_3 modes. However, this explanation and the mechanism illustrated in Figure 3 is based on the hypothesis that the most important factor contributing to the peak broadening is the collision between the ion cloud and the CRC gas, while the time required for the reaction taking place in the CRC and the subsequent acceleration of the newly created molecular ions and their transport out of the cell may also play an important role in the case of the mass-shift approach. When taking the combination of these two effects (collision and reaction) into account, a longer signal duration would be expected for the latter approach, while the experimental data rather show a longer signal duration in the case of on-mass monitoring (at 1 % of the peak height). It should however be taken into account that this observation might be the result of the lower sensitivity with

the mass-shift approach. The relatively low signal intensity observed in the NH_3 mass-shift approach makes it more difficult to distinguish the peak tail from the background signal. As a result, it cannot be excluded that the peak width at 1% of the peak height was underestimated. The larger standard deviations on the signal duration calculated for the NH_3 methods also indicate a higher variability between NP signals measured using NH_3, further supporting the different interactions between the ionic cloud and the reaction gas. The occurrence of this effect at an even larger magnitude might even split the population of a single NP event into various populations giving rise to partially overlapping peaks, thus having a strong influence on the accurate characterization of NPs *via* SP-ICP-MS (see section 3.3.).

3.1.2. Effect of gas flow rate

3.1.2.1. Effect of NP size

In addition to the effect of different CRC modes, the gas pressure in the CRC or the gas flow rate may also have an influence on the signal duration of single NP events. For evaluating this effect, Ag particles of different sizes (50, 75, 80, 100 and 200 nm) were measured using a single-quadrupole ICP-MS instrument equipped with a quadrupole CRC pressurized with He at different gas flow rates (0, 1, 2, 3, 4 and 5 mL min^{-1}). **Figure 4A** shows the signal duration as a function of the He gas flow rate for all Ag particle sizes studied. As can be seen, no significant differences in signal duration were observed in the absence of He ("no gas" mode – signal durations ranging from 0.76 to 0.81 ms, expressed as peak width at 1% of the maximum height), except in the case of 50 nm AgNPs for which a slightly shorter duration (0.62 ms) was found compared to all the other sizes. It needs to be noted, though, that the intensities of the NP spikes generated by 50 nm AgNPs were relatively low (7.2 counts at the maximum of the peak on average), so that the proximity to the LOD_{size} may compromise the accuracy of the signal duration measurements (see section 2.3.). **Figure 4A** indicates that the addition of He into the CRC increases the average signal duration of individual NP events

proportionally to the gas flow rate for all the particle sizes, thus supporting the hypothesis of collisions between the ion cloud and the CRC gas as reason for the anomalously wide peak profiles (see **Figure 3**). In addition, **Figure 4B** shows the increase in particle event signal durations at 5 mL min^{-1} of He compared to 0 mL min^{-1} of He for the AgNPs of several sizes. The signal durations were established to be higher by a factor of 1.31, 1.44, 1.65, 2.25 and 2.95 at 5 mL min^{-1} He than in no gas mode for particles of 50, 75, 80, 100 and 200 nm, respectively. Interestingly, these results clearly demonstrate that also the particle size has an important influence on the extent of the effect exerted by using CRC technology on the signal duration of NP events. This different behavior for particles as a function of their size can most likely be explained by the denser ion cloud formed for the larger particles, thus increasing the probability of interactions with the cell gas. Thus, in addition to the CRC mode, type of gas and gas flow rate, attention also needs to be paid to the size of the particles prior to SP-ICP-MS analysis using CRC technology to overcome spectral overlap (see Section 3.3.).

3.1.2.2. Effect of NP type

To assess the potential effect of the chemical composition of the NPs, the signal durations for 50 and 100 nm AuNPs and for 50 and 70 nm PtNPs were measured under the same conditions as described in the previous section, *i.e.*, He gas flow rates ranging from 0 to 5 mL min^{-1}, and the results thus obtained were compared with those of AgNPs. In this way, we aimed at assessing the potential differences in peak width for individual NPs with a different chemical composition, but with approximately the same diameter (Ag, Au and Pt NPs of 50 nm, Ag and Pt NPs of 70 and 75 nm, respectively, and Ag and Au NPs of 100 nm). **Figures 5A** (Ag and Au NPs) and **5B** (Ag and Pt NPs) show the effect of increasing the He flow rate on the signal duration for the different NP types. It is interesting to note that the results obtained in this experiment for 50 nm AuNPs using a single-quadrupole ICP-MS instrument equipped with a quadrupole CRC (0.62 ± 0.19 and 0.79 ± 0.25 for 0 and 5 mL min^{-1} He, respectively) are not significantly different from those reported in section 3.1.1.

for the same AuNPs using a tandem ICP-MS instrument equipped with an octopole CRC (0.60 ± 0.10 and 0.74 ± 0.13 for 0 and 5 mL min^{-1} He, respectively). Self-evidently, the influence of different types of mass spectrometers and/or of CRC technologies on the transit time of the ion cloud generated by individual NPs merits further study, but these results seem to indicate that the effect of introducing an additional quadrupole and/or of using a different type of CRC (quadrupole *vs* octopole) might be negligible compared to the effect of adding a CRC gas.

In the comparison of different NP types, on the one hand, very similar results were obtained for Ag and Au NPs, both in terms of average signal duration and effect of the He flow rate. On the other hand, significantly shorter peak widths were found for PtNPs compared to AgNPs and AuNPs of the same size, while the effect of increasing the He flow also seemed less pronounced. In a previous work, Kéri *et al*.**[43]** reported significantly longer signal durations for AuNPs than for AgNPs and tried to attribute this difference to physical processes that can influence the transit time of the ion cloud (*e.g.*, temperature and enthalpy of melting and boiling, and/or ionization energy). However, all physical processes studied suggested that AgNPs should produce longer transient times than AuNPs, and it was concluded that, most likely, some effects occurring in the plasma (*e.g.*, charge-transfer reactions) can also contribute. In this work, the significant differences observed for PtNPs do not seem to be related with, *e.g.*, ionization energy (Au > Pt > Ag). In addition to the physicochemical properties of the constituting element, also the morphology of the NPs may influence the signal duration of single NP events. In order to shed light onto these differences, TEM images of Ag, Au and Pt NPs were obtained, as shown in **Figure 6**. Interestingly, it was found that – in contrast to Ag and Au NPs – both 50 and 70 nm PtNPs were agglomerates of NPs of approximately 1 – 2 nm. This different morphology can be the cause of the significantly shorter signal duration established for PtNPs, although the influence of a different chemical composition and thus, different physicochemical properties cannot be ruled out. Ag and Au NPs showed a similar behavior, but both are spherical and metallic NPs from the same group within the periodic table. Thus, they are expected to have rather similar chemical and physical properties. In the case of PtNPs, we cannot

assess the influence of the difference in chemical composition as the aberrant behavior can most likely be attributed to the different morphology. Based on these results, we cannot provide a full description of how NP type (composition) affects the signal duration of a single NP event, but our results suggest that the use of the temporally resolved information generated by SP-ICP-MS could also provide some nano-morphological information.

3.2. Characterization of Fe_3O_4 NPs via SP-ICP-MS/MS operated in different CRC modes

3.2.1. Method development for interference-free determination of Fe using CRC technology and ICP-MS/MS

As a result of their unique physical and chemical properties, iron nanoparticles (FeNPs) are of the utmost interest for environmental and biological applications.**[46-48]** However, the characterization of FeNPs by SP-ICP-MS is hampered by the occurrence of interfering ions, such as the ubiquitous ArO^+ polyatomic ions with the same nominal m/z ratio as the most abundant Fe isotope (56, relative isotopic abundance of 91.75%), thus requiring the development of powerful ICP-MS methods able to address this problem of spectral overlap. Two strategies were developed for this purpose, (1) an ICP-MS/MS mass-shift approach based on the formation of an NH_3-based reaction product ion ($Fe(NH_3)_x^+$) and (2) an ICP-MS/MS on-mass approach using H_2 as CRC gas (measurement of Fe^+ ions at their original m/z ratio). In both cases, effective removal of the ArO^+ polyatomic interference can be achieved, according to the following reactions:

(1) $Fe^+ + NH_3 \rightarrow Fe(NH_3)_x^+$ (cluster formation – reaction mode)

$ArO^+ + NH_3 \rightarrow ArO + NH_3^+$ (charge transfer)

(2) $Fe^+ + H_2 \rightarrow Fe^+ + H_2$ (no reaction)

$ArO^+ + H_2 \rightarrow ArOH^+ + H$ (H addition – reaction mode)

$ArO^+ + H_2 \rightarrow ArO^+ + H_2$ (collision followed by kinetic energy discrimination – KED mode)

In the first case, product ion scans were performed at different gas flow rates (between 1 and 5 mL min^{-1}, see **Figure 7A**), and $Fe(NH_3)_2^+$ at m/z = 90 amu was identified as the best suited reaction product ion. Maximum sensitivity was obtained at 3 mL min^{-1} of NH_3 (mixture of 10% NH_3 in He). For the H_2 on-mass approach, a gas flow rate of 6.5 mL min^{-1} of H_2 was selected after optimization of the signal-to-background ratio (see **Figure 7B**). It needs to be noted that, after optimization, the sensitivity of the two methods developed was approximately 110 000 cps per 1 µg L^{-1} of an ionic standard solution of Fe.

In addition, also the effect of using the axial acceleration (AA) option available for the Agilent 8900 ICP-MS/MS instrument was evaluated in the case of the NH_3 mass-shift approach. The AA function allows a voltage gradient to be applied to accelerate ions along the ion guide axis of the octopole, providing an enhanced sensitivity when operating an ICP-MS/MS instrument in reaction cell mode. This counteracts the relatively low kinetic energy of newly created reaction product ions, reducing ion transmission efficiency due to collisional scattering or space charge repulsion. The axial acceleration voltage increases the kinetic energy of those reaction product ions, thus enhancing their transport out of the cell and into the second quadrupole.**[49]** We studied the influence of AA on the signal intensities of the reaction product ion selected at different gas flow rates by varying the AA voltage between -2 and +2 V (a summary of these results is visualized in **Figure 8**). It was observed that the optimum AA voltage increases with the increase of the gas flow rate (0.0, 0.1, 0.2, 0.5 and 1 V at 1, 2, 3, 4 and 5 mL min^{-1} NH_3, respectively). Based on these results, it was demonstrated that the use of higher gas flow rates in the CRC reduces the ion transmission efficiency of the reaction product ions, thus necessitating a higher AA voltage to compensate for this effect. After optimization of the AA, the highest signal intensity for $Fe(NH_3)_2^+$ was found at 3 mL min^{-1} of NH_3 and an AA setting of 0.2 V (120 000 cps per 1 µg L^{-1} Fe). In this specific case, the operation of the ICP-MS/MS instrument with the AA off resulted in a reduction of the sensitivity (ion transmission efficiency) by a factor of ~2.

3.2.2. *Effect of using CRC technology on the SP-ICP-MS analysis of 50 and 200 nm Fe_3O_4 NPs*

The two methods developed (based on H_2 on-mass monitoring and an NH_3 mass-shift approach, respectively) were subsequently used to study the effect of using the CRC technology on the characterization of 50 and 200 nm Fe_3O_4 NPs by means of SP-ICP-MS/MS. Both methods provide approximately the same sensitivity for the interference-free determination of ^{56}Fe, and thus, they are *a priori* also expected to provide approximately the same NP detection capabilities when operating the ICP-MS/MS instrument in SP mode. However, while in the case of the H_2 on-mass approach, the signal spikes corresponding to individual NP events were found to be clearly separated from the background (ionic) signal for both 50 and 200 nm Fe_3O_4 NPs, the use of NH_3 mass-shift did not allow to distinguish the 50 nm Fe_3O_4 NP spikes from the background signal. As can be seen from **Figure 9** (depicting the signal for individual events for Fe_3O_4NPs of 200 nm), this can be attributed to the effect of using NH_3 on the signal shape and height. Since the sensitivities of the H_2 on-mass and NH_3 mass-shift methods were approximately the same (see section 3.3.1.), the lower maximum peak height obtained for the same NPs using the NH_3-based method (160 counts) compared to that of H_2 (1500 counts) can only be explained by the more pronounced peak broadening, as already shown in section 3.1.1. In contrast to the significant differences in peak height, the peak areas calculated using the HDIP software corresponded to 3900 and 3700 counts for H_2 and NH_3, respectively. In addition, it needs to be pointed out that the use of AA did not improve the situation, as similar peak widths were obtained when operating the ICP-MS/MS instrument with AA on/off.

In this case, a very pronounced peak broadening was observed as a result of the combination of (*i*) the use of NH_3 gas (see section 3.1.1) and (*ii*) the measurement of relatively large particles (200 nm, see section 3.1.2.1.). As a result of these two effects, an average signal duration of 6.10 ± 1.60 ms was calculated for 200 nm Fe_3O_4 NPs using the NH_3 mass-shift approach, while for the same NPs, the average signal duration was only 0.94 ± 0.49 ms when using the H_2 on-mass method (see **Figure 9**). **Figure 10** shows the size distribution for 50 and 200 nm Fe_3O_4 NPs. It is clear that the very pronounced increase in signal duration induced by the introduction of NH_3 gas into the CRC of an ICP-

MS/MS instrument has a detrimental effect on the NP detection capabilities and it even precludes measuring 50 nm Fe_3O_4 NPs using this approach, despite of the lower effect expected for 50 nm compared to 200 nm NPs. In this context, it needs to be noted that the NH_3 flow rate was optimized to achieve the highest signal-to-background ratio for ionic Fe, as this can be seen as the most commonly used tuning approach. However, this selection of NH_3 gas flow rate clearly compromises the NP detection capabilities due to the significant peak broadening induced by this relatively high gas flow rate. In other words, it can be assumed that these circumstances do not always provide the best NP detection capabilities. In order to obtain further insight, the effect of using lower NH_3 gas flow rates (1.0, 1.5, 2.0, 2.5 and 3.0 mL min^{-1}) on the detectability of 50 nm Fe_3O_4 NPs was evaluated. Unfortunately, none of the conditions selected allowed us to detect 50 nm Fe_3O_4 NPs, as in the case of this specific reaction, a reduction in the NH_3 gas flow rate also strongly decreases the reaction efficiency and thus, the sensitivity.

For 50 nm (H_2) and 200 nm (H_2 and NH_3), a very good agreement between the size distribution obtained using SP-ICP-MS/MS and the TEM results provided by the manufacturer was obtained. However, comparison of the size distribution for the 200 nm Fe_3O_4 NPs using both approaches showed a slightly wider distribution for the NH_3-based method compared to the use of H_2, while also NPs with sizes exceeding 300 nm appear when using the NH_3 mass-shitt approach. This can also be attributed to the larger signal duration and the higher probability of overlap of peaks corresponding to individual NPs, as will be discussed in the next section. In a previous work, we saw that the use of CH_3F as a reaction gas for the interference-free determination of SiO_2 NPs also resulted in wider size distributions for the larger particles (300 and 400 nm) compared to the use of H_2.**[50]** In that work, an Agilent 8800 ICP-MS/MS instrument was used and as the minimum dwell time with this instrument is limited to 3 ms, we could not further study the differences between both approaches, but the longer signal duration of individual NP events using CH_3F is most likely the explanation for those differences.

3.3. Influence of the signal duration on the accuracy of the SP-ICP-MS measurements

The increase of the transit time of the NP ion cloud as a result of the use of CRC technology in ICP-QMS instrumentation exerts a detrimental effect on the SP-ICP-MS analysis, thus necessitating the application of some additional measures to minimize the consequences in terms of accuracy of the NP size, particle number density and mass concentration results. The occurrence of double events might be seen as one of the consequences of an anomalously high NP signal duration. In SP-ICP-MS, the NPs are randomly distributed in the diluted aqueous solutions, and this solution should be sufficiently diluted to avoid two or more particles being detected at the same time. Poisson statistics can be used to estimate the probability of one or more than one particle reaching the plasma in a fixed time interval:**[9, 15, 17, 18]**

$$P_x = \frac{\lambda^x}{x!} e^{-\lambda}$$

where x is the number of particles and λ is the number of particles entering the plasma in a fixed period of time (= nanoparticle flux, Q_{NP}). λ can be calculated using the following equation:

$$\lambda = Q_{NP} \times t = C_{NP} \times Q_{sam} \times \eta_{neb} \times t$$

C_{NP} is the particle number density, Q_{sam} is the sample flow rate, η_{neb} is the nebulization efficiency and t is the fixed period of time. This time has been considered as the dwell time (t_{dwell}) when working in the millisecond range, and as the peak width of the transient signal (w_{peak}) when working in the microsecond range (generally established at 0.5 ms). However, the assumption of a signal duration of ~0.5 ms is not valid when using CRC technology to avoid spectral overlap, as demonstrated in the previous sections. The peak widths obtained using this approach can range from 0.5 to 6 ms depending on the size of the NP and the type of CRC gas and the flow rate at which it is introduced into the CRC. In order to further illustrate the effect of this longer signal durations on the probability of more than one event occurring within the same time interval (particle coincidence), the probabilities were calculated at different NP fluxes (5, 20 and 50 s^{-1}) and peak widths (0.5, 1, 2.5 and 5 ms) based on Poisson statistics and the corresponding results are shown in **Table 2**. It can be seen

that for conventional NP fluxes, for instance 20 Hz, the probability of particle coincidence increases approximately 2 orders of magnitude for NP events with a peak width of 5 ms compared to 0.5 ms.

This increase in the probability of particle coincidence will result in an underestimation of the particle number density and an overestimation of the NP size. Depending on the type of software used for NP data treatment, two individual NP events can be resolved, even if they partially overlap (see **Figure 11A**). In this specific case, accurate results can still be achieved for the particle number density, but incomplete peak areas will lead to inaccurate NP sizes and mass concentrations. A further refinement of this approach would lie in deconvolution of overlapping peaks, although the asymmetry of the NP peaks poses additional challenges.**[51]** Therefore, an estimation of the signal duration of individual NP events prior to SP-ICP-MS using CRC technology is recommended in order to select an appropriate dilution factor. However, this approach requires an increase of the measurement time to avoid inaccurate results because of poor counting statistics.

In addition to the occurrence of particle coincidence, the SP detection capabilities (LOD_{size}) can also be affected by pronounced peak broadening (see **Figure 11B**). The overlap of the signal from the NP with that of the background can potentially hamper the detection of the smallest NPs. As a result, the average NP size determined could be biased high, while an inaccurate particle number density will be obtained as a result of the counting of the larger NPs only.

In addition to the direct effect on the accuracy of the NP characterization, it needs to be noted that the use of some approaches reported on in the literature to calibrate the NP size based on the use of the NP signal durations can also be affected when using CRC technology.**[43]** If such approaches are intended, it has to be considered that the duration depends on the size and the collisions/interactions between the ion cloud and the CRC gas, and thus, higher variations are expected.

Finally, also a positive side effect of the increase in signal duration for NP events using CRC technology can be noted. This strategy can be used to monitor multiple (≥2) nuclides in SP mode.

Montaño *et. al.* have reported the use of microsecond dwell times for the detection of two elements in the same nanoparticle, although the relatively short signal duration of individual NP events and the necessity of working with a sufficiently high settling time to account for ion flight time through the quadrupole and the detector (~100 µs) leads to a poor definition of the peak shape (generally only 1 data point to define the maximum of the peak).**[38]** This temporal resolution can clearly be improved by using CRC technology, as is clearly illustrated in **Figure 9**, for which the maximum of the peak using the H_2 on-mass approach is defined by 1 data point (100 µs) only, in contrast to the NH_3 mass-shift approach, for which the maximum of the peak is defined by at least 5 data points (500 µs). Obviously, there is a trade-off in terms of size detectability, but there are situations where this longer NP peak width can be beneficial and used for multi-nuclide monitoring using a sequential mass spectrometer in the context of (*i*) cross-validation of the results using two isotopes from the same element, (*ii*) measurement of bimetallic NPs (with a core of one metal and a shell of another) and (*iii*) use of isotope dilution as a calibration strategy. Self-evidently, the use of the quasi-simultaneous detection capabilities provided by time-of-flight ICP-MS (ICP-TOFMS) instrumentation provides far greater capabilities for multi-isotope monitoring in this context.**[52-54]**

4. CONCLUSION

The use of CRC technology in SP-ICP-MS with quadrupole-based instrumentation is mandatory for those NPs strongly affected by the occurrence of spectral overlap (*e.g.*, Fe_3O_4 NPs). However, this work has demonstrated (using two different instrument types) that the introduction of a gas into the CRC has an important effect on the signal duration of a single NP event. The use of different CRC modes revealed that gases with a larger collisional cross-section (*e.g.*, NH_3) induce a more pronounced peak broadening than gases with a smaller one do (*e.g.*, He and H_2). In addition, the gas pressure in the CRC (determined by the gas flow rate) and even the type and morphology of the NPs might influence the transit time of the NP ion cloud though the mass spectrometer. These

conclusions have been further illustrated by the characterization of Fe_3O_4 NPs, which are strongly affected by the occurrence of spectral interference. The detrimental effect of using an NH_3 mass-shift approach did not enable 50 nm Fe_3O_4 NPs to be distinguished from the background signal, while this was not found to be the case when using a H_2 on-mass approach. The effect was found to be most pronounced for larger particles, and thus, the characterization of NPs of smaller dimensions are less affected by the use of CRC technology. To minimize the effect for larger particles, light gases and low gas flow rates are recommended. In addition, the effect of a longer NP signal width on the accuracy of the SP-ICP-MS measurements, such as higher probability of particle coincidence, higher LOD_{sizes}, and inaccurate size distribution, particle number density and mass concentration results has been described into detail. This effect, however, can also be exploited for multi-isotope monitoring using sequential ICP-MS instrumentation operated in SP mode.

ACKNOWLEDGMENTS

Eduardo Bolea-Fernandez thanks BOF-UGent for his postdoctoral grant. Tong Liu thanks BOF-UGent for her PhD grant. The authors acknowledge the funding obtained *via* CTQ2015-64684P (MINECO/FEDER) from the Aragón Government (Fondo Social Europeo) and *via* PGC2018-093753-B-I00 (MCIU/AEI//FEDER, UE). This work was supported by CNPq, Conselho Nacional de Desenvolvimiento Científico e Tecnológico – Brazil (232487/2014-6). Frank Vanhaecke acknowledges the Special Research fund of Ghent University BOF-UGent for financial support. The TEM measurements have been conducted in the "Laboratório de Microscopias Avanzadas" at "Insituto de Nanociencia de Aragón – Universidad de Zaragoza". LMA-INA is acknowledged for offering access to their instruments and expertise. Agilent Technologies is acknowledged for providing access to Agilent 8900 ICP-MS/MS instrumentation. The authors also would like to thank Stijn J. M. Van Malderen for his help with the use of the HDIP software.

REFERENCES

[1] J.R. Peralta-Videa, L. Zhao, M.L. Lopez-Moreno, G. de la Rosa, J. Hong, J.L. Gardea-Torresdey, Nanomaterials and the environment: A review for the biennium 2008-2010, J. Hazard. Mater. 186 (2011) 1 - 15.

[2] L. Calzolai, D. Gilliland, F. Rossi, Measuring nanopaticles size distribution in food and consumer products: a review, Food Addit. Contam., Part A 29 (2012) 1183 - 1193.

[3] M.R. Wiesner, G.V. Lowry, P. Alvarez, D. Dionysiou, P. Biswas, Assessing the risks of manufactured nanomaterials, Environ. Sci. Technol. 40 (2006) 4336 - 4345.

[4] M. Hassellöv, J.W. Readman, J.F. Ranville, K. Tiede, Nanoparticle analysis and characterization methodologies in environmental risk assessment of engineered nanoparticles, Ecotoxicology 17 (2008) 344 - 361.

[5] F. Laborda, E. Bolea, G. Cepriá, M.T. Gómez, M.S. Jiménez, J. Pérez-Arantegui, J.R. Castillo, Detection, characterization and quantification of inorganic engineered nanomaterials: A review of techniques and methodological approaches for the analysis of complex samples, Anal. Chim. Acta 904 (2016) 10 - 32.

[6] M.S. Jiménez, M.T. Gómez, E. Bolea, F. Laborda, J. Castillo, An approach to the natural and engineered nanoparticles analysis in the environment by inductively coupled plasma mass spectrometry, Int. J. Mass Spectrom. 307 (2011) 99 - 104.

[7] F. Laborda, J. Jiménez-Lamana, E. Bolea, J.R. Castillo, Selective identification, characterization and determination of dissolved silver (I) and silver nanoparticles based on single particle detection by inductively coupled plasma mass spectrometry, J. Anal. At. Spectrom. 26 (2011) 1362 - 1371.

[8] H.E. Pace, N.J. Rogers, C. Jarolimek, V.A. Coleman, C.P. Higgins, J.F. Ranville, Determining Transport Efficiency for the Purpose of Counting and Sizing Nanoparticles via Single Particle Inductively Coupled Plasma Mass Spectrometry, Anal. Chem. 83 (2011) 9361 - 9369.

[9] H.E. Pace, N.J. Rogers, C. Jarolimek, V.A. Coleman, E.P. Gray, C.P. Higgins, J.F. Ranville, Single Particle Inductively Coupled Plasma-Mass Spectrometry: A Performance Evaluation and Method Comparison in the Determination of Nanoparticle Size, Environ. Sci. Technol. 46 (2012) 12272 - 12280.

[10] F. Laborda, E. Bolea, J. Jiménez-Lamana, Single Particle Inductively Coupled Plasma Mass Spectrometry: A Powerful Tool for Nanoanalysis, Anal. Chem. 86 (2014) 2270 - 2278.

[11] C. Degueldre, P.-Y. Favarger, Colloid analysis by single particle inductively coupled plasma-mass spectroscopy: a feasibility study, Colloids Surf., A 217 (2003) 137 - 142.

[12] M.D. Montaño, J.W. Olesik, A.G. Barber, K. Challis, J.F. Ranville, Single Particle ICP-MS: Advances toward routine analysis of nanomaterials, Anal. Bioanal. Chem. 408 (2016) 5053 - 5074.

[13] B. Meermann, V. Nischwitz, ICP-MS for the analysis at the nanoscale - a tutorial review, J. Anal. At. Spectrom. 33 (2018) 1432 - 1468.

[14] S. Gschwind, L. Flamigni, J. Koch, O. Borovinskaya, S. Groh, K. Niemax, D. Günther, Capabilities of inductively coupled plasma mass spectrometry for the detection of nanoparticles carried by monodisperse microdroplets, J. Anal. At. Spectrom. 26 (2011) 1166 - 1174.

[15] J.W. Olesik, P.J. Gray, Considerations for measurement of individual nanoparticles or microparticles by ICP-MS: determination of the number of particles and the analyte mass in each particle, J. Anal. At. Spectrom. 27 (2012) 1143 - 1155.

[16] J. Tuoriniemi, G. Cornelis, M. Hassellöv, Improving the accuracy of single particle ICPMS for measurement of size distributions and number concentrations of nanoparticles by determining analyte partitioning during nebulization, J. Anal. At. Spectrom. 29 (2014) 743 - 752.

[17] I. Abad-Álvaro, E. Peña-Vázquez, E. Bolea, P. Bermejo-Barera, J.R. Castillo, F. Laborda, Evaluation of number concentration quantification by single-particle inductively coupled plasma mass spectrometry: microsecond vs. millisecond dwell times, Anal. Bioanal. Chem. 408 (2016) 5089 - 5097.

[18] F. Laborda, J. Jiménez-Lamana, E. Bolea, J.R. Castillo, Critical considerations for the determination of nanoparticle number concentrations, size and number size distributions by single particle ICP-MS, J. Anal. At. Spectrom. 28 (2013) 1220 - 1232.

[19] I. Kálomista, A. Kéri, G. Galbács, On the applicability and performance of the single particle ICP-MS nano-dispersion characterization method in cases complicated by spectral interferences, J. Anal. At. Spectrom. 31 (2016) 1112 - 1122.

[20] L. Fréchette-Viens, M. Hadioui, K.J. Wilkinson, Practical limitations of single particle ICP-MS in the determination of nanoparticles size distributions and dissolution: case of rare earth oxides, Talanta 163 (2017) 121 - 126.

[21] N. Jakubowski, L. Moens, F. Vanhaecke, Sector field mass spectrometers in ICP-MS, Spectrochim. Acta, Part B 53 (1998) 1739 - 1763.

[22] N. Jakubowski, T. Prohaska, L. Rottmann, F. Vanhaecke, Inductively Coupled Plasma - and Glow Discharge Plasma - Sector Field Mass Spectrometry Part I: Tutorial: Fudamentals and instrumentation, J. Anal. At. Spectrom. 26 (2011) 693 - 726.

[23] J. Tuoriniemi, G. Cornelis, M. Hassellöv, A new peak recognition algorithm for detection of ultra-small nano-particles by single particle ICP-MS using rapid time resolved data acquisition on a sector-field mass spectrometer, J. Anal. At. Spectrom. 30 (2015) 1723 - 1729.

[24] P. Shaw, A. Donard, Nano-particle analysis using dwell times between 10 µs and 70 µs with an upper counting limit of greater than 3 x 10^7 cps and a gold nanoparticle detection limit of less than 10 nm diameter, J. Anal. At. Spectrom. 31 (2016) 1234 - 1242.

[25] K. Newman, C. Metcalfe, J. Martin, H. Hintelmann, P. Shaw, A. Donard, Improved single particle ICP-MS characterization of silver nanoparticles at environmentally relevant concentrations, J. Anal. At. Spectrom. 31 (2016) 2069 - 2077.

[26] R. Peters, Z. Herrera-Rivera, A. Undas, M. van der Lee, H. Marvin, H. Bouwmeester, S. Weigel, Single particle ICP-MS combined with a data evaluation tool as a routine technique for the analysis of nanoparticles in complex matrices, J. Anal. At. Spectrom. 30 (2015) 1274 - 1285.

[27] M. Tharaud, A.P. Gondikas, M.F. Benedetti, F.von der Kammer, T. Hofmann, G. Cornelis, TiO_2 nanomaterial detection in calcium rich matrices by spICPMS. A matter of resolultion and treatment, J. Anal. At. Spectrom. 32 (2017) 1400 - 1411.

[28] D.R. Bandura, V.I. Baranov, S.D. Tanner, Reaction chemistry and collisional processes in multipole devices for resolving isobaric interferences in ICP-MS, Fresenius' J. Anal. Chem. 370 (2001) 454 - 470.

[29] B. Hattendorf, D. Günther, Suppression of in-cell generated interferences in a reaction cell ICP-MS by bandpass tuning and kinetic energy discrimination, J. Anal. At. Spectrom. 19 (2004) 600 - 606.

[30] S. Diez Fernández, N. Sugishama, J. Ruiz Encinar, A. Sanz-Medel, Triple Quad ICP-MS (ICPQQQ) as a New Tool for Absolute Quantitative Proteomics and Phosphoproteomics, Anal. Chem. 84 (2012) 5851 - 5857.

[31] L. Balcaen, E. Bolea-Fernandez, M. Resano, F. Vanhaecke, Inductively coupled plasma-Tandem mass spectrometry (ICP-MS/MS): A powerful and universal tool for the interference-free determination of (ultra)trace elements - A tutorial review, Anal. Chim. Acta 894 (2015) 7 - 19.

[32] N. Yamada, Kinetic energy discrimination in collision/reaction cell ICP-MS: Theoretical review of principles and liminations, Spectrochim. Acta, Part B 110 (2015) 31 - 44.

[33] A. Virgilio, R.S. Amais, C.D.B. Amaral, L.L. Fialho, D. Schiavo, J.A. Nóbrega, Reactivity and analytical performance of oxygen as cell gas in inductively coupled plasma tandem mass spectrometry, Spectrochim. Acta, Part B 126 (2016) 31 - 36.

[34] E. Bolea-Fernandez, L. Balcaen, M. Resano, F. Vanhaecke, Overcoming spectral overlap *via* inductively coupled plasma-tandem mass spectrometry (ICP-MS/MS). A tutorial review, J. Anal. At. Spectrom. 32 (2017) 1660 - 1679.

[35] B. Klencsár, C. Sánchez, L. Balcaen, J. Todolí, F. Lynen, F. Vanhaecke, Comparative evaluation of ICP sample introduction systems to be used in the metabolite profiling of chlorine-containing pharmaceuticals via HPLC-ICP-MS, J. Pharm. Biomed. Anal. 153 (2018) 135 - 144.

[36] S.J.M. Van Malderen, A.J. Managh, B.L. Sharp, F. Vanhaecke, Recent developments in the design of rapid response cells for laser ablation-inductively coupled plasma-mass spectrometry and their impact on bioimaging applications, J. Anal. At. Spectrom. 32 (2016) 423 - 439.

[37] A. Hineman, C. Stephan, Effect of dwell time on single particle inductively coupled plasma mass spectrometry data acquisition quality, J. Anal. At. Spectrom. 29 (2014) 1252 - 1257.

[38] M.D. Montaño, H.R. Badiei, S. Bazargan, J.F. Ranville, Improvements in the detection and characterization of engineered nanoparticles using spICP-MS with microsecond dwell times, Environ. Sci.: Nano 1 (2014) 338 - 346.

[39] J. Liu, K.E. Murphy, R.I. MacCuspie, M.R. Winchester, Capabilities of Single Particle Inductively Coupled Plasma Mass Spectrometry for the Size Measurement of Nanoparticles: A Case Study on Gold Nanoparticles, Anal. Chem. 86 (2014) 3405 - 3414.

[40] M.D. Montaño, B.J. Majestic, A.K. Jämting, P. Westerhoff, J.F. Ranville, Methods for the Detection and Characterization of Silica Colloids by Microsecond spICP-MS, Anal. Chem. 88 (2016) 4733 - 4741.

[41] I. Strenge, C. Engelhard, Capabilities of fast data acquisition with microsecond time resolution in inductively coupled plasma mass spectrometry and identification of signal artifacts from millisecond dwell times during detection of single gold nanoparticles, J. Anal. At. Spectrom. 31 (2016) 135 - 144.

[42] L.A. Simpson, M. Thomsen, B.J. Alloway, A. Parker, A dynamic reaction cell (DRC) solution to oxide-based interferences in inductively coupled plasma mass spectrometry (ICP-MS) analysis of the noble metals, J. Anal. At. Spectrom. 16 (2001) 1375 - 1380.

[43] A. Kéri, I. Kálomista, D. Ungor, A. Bélteki, E. Csapó, I. Dékány, T. Prohaska, G. Galbács, Determination of the structure and composition of Au-Ag bimetallic spherical nanoparticles using single particle ICP-MS measurements performed with normal and high temporal resolution, Talanta 179 (2018) 193 - 199.

[44] J. Fuchs, M. Aghaei, T.D. Schachel, M. Sperling, A. Bogaerts, U. Karst, Impact of the Particle Diameter on Ion Cloud Formation from Gold Nanoparticles in ICPMS, Anal. Chem. 90 (2018) 10271 - 10278.

[45] I.I. Stewart, J.W. Olesik, Time-resolved measurements with single droplet introduction to investigate space-charge effects in plasma mass spectrometry, J. Am. Soc. Mass Spectrom. 10 (1999) 159 - 174.

[46] A.K. Gupta, M. Gupta, Synthesis and surface engineering of iron oxide nanoparticles for biomedical applications, Biomaterials 26 (2005) 3995 - 4021.

[47] P. Xu, G.M. Zeng, D.L. Huang, C.L. Feng, S. Hu, M.H. Zhao, C. Lai, Z. Wei, C. Huang, G.S. Xie, Z.F. Liu, Use of iron oxide nanomaterials in wastewater treatment: a review, Sci. Total Environ. 424 (2012) 1 - 10.

[48] J. García-Fernández, C. Sánchez-González, J. Bettmer, J. Llopis, N. Jakubowski, U. Panne, M. Montes-Bayón, Quantitative assessment of the metabolic products of iron oxide nanoparticles to be used as iron supplements in cell cultures, Anal. Chim. Acta 1039 (2018) 24 - 30.

[49] A. Technologies, Agilent 8900 Triple Quadrupole ICP-MS. Technical Overview, http://hpst.cz/sites/default/files/attachments/5991-6942en-8900-icp-qqq-tech-overview-final.pdf (accessed January 2019).

[50] E. Bolea-Fernandez, D. Leite, A. Rua-Ibarz, L. Balcaen, M. Aramendía, M. Resano, F. Vanhaecke, Characterization of SiO_2 nanoparticles by single particle-inductively coupled plasma-tandem mass spectrometry (SP-ICP-MS), J. Anal. At. Spectrom. 32 (2017) 2140 - 2152.

[51] G. Cornelis, M. Hassellöv, A signal deconvolution method to discriminate smaller nanoparticles in single particle ICP-MS, J. Anal. At. Spectrom. 29 (2014) 134 - 144.

[52] O. Borovinskaya, B. Hattendorf, M. Tanner, S. Gschwind, D. Günther, A prototye of a new inductively coupled plasma time-of-flight mass spectrometer providing temporally resolved, multi-element detection of short signals generated by single particles and droplets, J. Anal. At. Spectrom. 28 (2013) 226 - 233.

[53] A. Praetorius, A. Gundlach-Graham, E. Goldberg, W. Fabienke, J. Navratilova, A. Gondikas, R. Kaegi, D. Günther, T. Hofmann, F.von der Kammer, Single-particle multi-element fingerprinting (spMEF) using inductively-coupled plasma time-of-flight mass spectrometry (ICP-TOFMS) to identify engineered nanoparticles against the elevated natural background in soils, Environ. Sci. Nano 4 (2017) 307 - 314.

[54] S. Naasz, S. Weigel, O. Borovinskaya, A. Serva, C. Cascio, A.K. Undas, F.C. Simeone, H.J.P. Marvin, R.J.B. Peters, Multi-element analysis of single nanoparticles by ICP-MS using quadrupole and time-of-flight technologies, J. Anal. At. Spectrom. 33 (2018) 835 - 845.

Figure captions:

Fig. 1 SP-ICP-MS data treatment using the in-house developed HDIP software. **Figures 1A** and **1B** show the raw data (intensity *vs* time) from one measurement replicate of a AuNP standard. **Figure 1C** illustrates the identification of the signal spikes corresponding to single NP events; the selection criterion was based on different parameters, such as a selected delta value, lower relative maximum threshold and higher relative minimum threshold. **Figure 1D** shows the average peak profile and the results obtained for the complete data set (peak profile, signal duration, number of peaks found, area average, *etc*). The red triangles highlight the peak maxima, while the integration intervals are visualized by green triangles.

Fig. 2 Effect of the different CRC modes on the signal duration and peak shape of individual NPs. In all cases, 50 nm AuNPs were measured, except for NH_3 mass-shift, for which 100 nm AuNPs were selected. The average normalized peak profile of approximately 1 000 NP events per CRC mode was calculated using the HDIP software. In the case of both NH_3 methods, a mixture of 10% NH_3 in He was used in combination with an extra flow of 1 mL min^{-1} He, as recommended by the instrument manufacturer.

Fig. 3 Graphical illustration of the effect of introducing a gas in the CRC of an ICP-CRC-QMS instrument on the NP signal duration of individual NP events. The graphic shows the disturbances in the ion cloud generated by individual NPs as a result of interactions with a gas in the CRC system and the thus caused effect on the NP signal distribution.

Fig. 4 A: Increase of the signal duration as a function of the He flow rate for AgNPs of various sizes ranging from 50 to 200 nm. **B:** Increase of the signal duration ratio (NP signal duration at 5 mL min^{-1} relative to that at 0 mL min^{-1}) for AgNPs with different sizes.

Fig. 5 Comparison of the signal duration of Ag and Au NPs (**Figure 5A**) and Ag and Pt NPs (**Figure 5B**) as a function of increasing He flow rates.

Fig. 6 TEM images obtained for 50 nm Ag, Au and Pt NPs. It can be observed that the PtNPs are agglomerates of NPs of approximately 1 – 2 nm.

Fig. 7 A: Search for the best suited $^{56}Fe(NH_3)_x^+$ reaction product ion (using a 1 µg L^{-1} Fe solution) at different gas flow rates using product ion scanning. **B:** Optimization of the H_2 gas flow rate for the on-mass measurement of $^{56}Fe^+$ using the ramp cell gas option: signal intensity for 1 µg L^{-1} Fe and background signal (left y-axis, logarithmic scale) and signal-to-background ratio (right y-axis).

Fig. 8 Effect of axial acceleration (AA) on the intensity of the reaction product ion selected ($^{56}Fe(NH_3)_2^+$).

Fig. 9 Effect of the use of H_2 on-mass and NH_3 mass-shift approaches on the signal duration and peak shape of 200 nm Fe_3O_4 NPs. The average peak profile of approximately 1 000 NP events per CRC mode was calculated using the HDIP software.

Fig. 10 Size distribution of 50 (H_2 – A) and 200 (H_2 – B and NH_3 – C) nm Fe_3O_4 NPs using SP-ICP-MS/MS. The TEM size distributions were provided by the manufacturer.

Fig. 11 (A) Probability of occurrence of double events (particle coincidence) as a function of the signal duration of individual NP events and (B) effect of signal broadening on the accuracy of NP characterization and their LOD_{size}.

Fig. 1

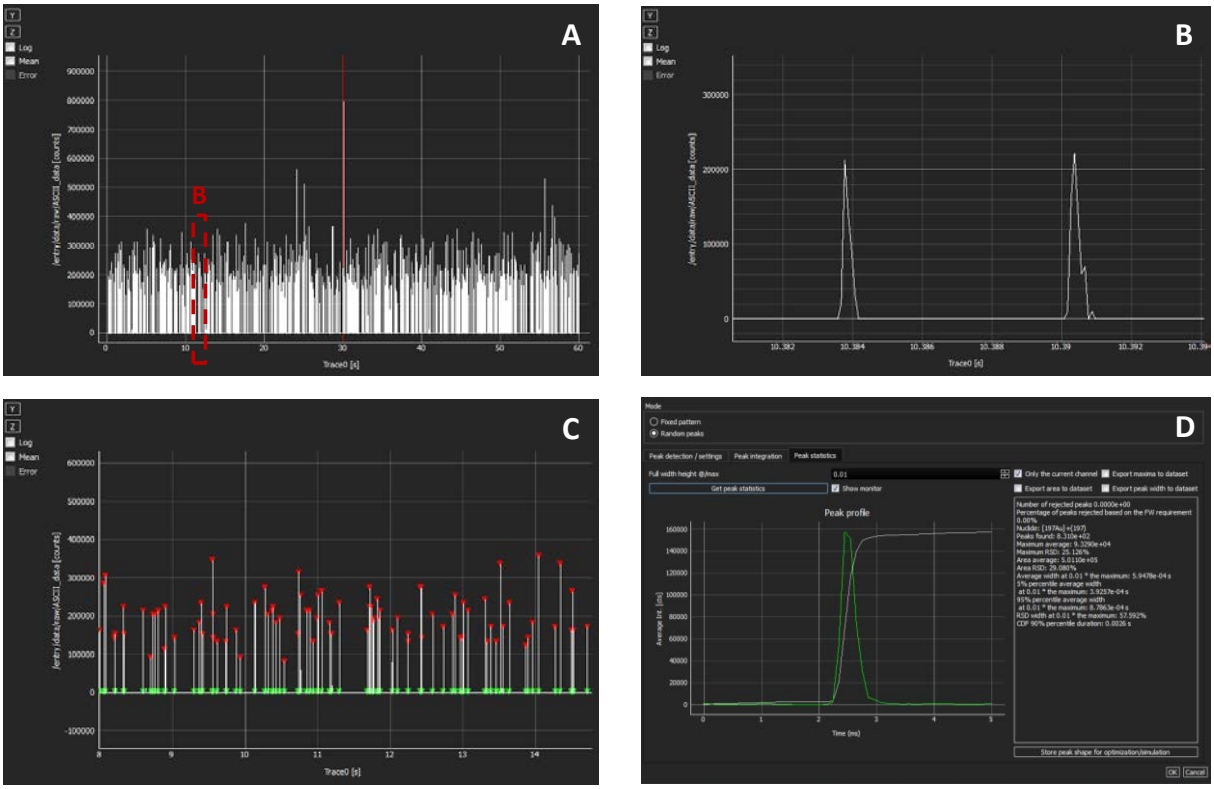
A
B
C
D
Log
Mean
Error
Trace0 [s]
Peak profile
Fixed pattern
Random peaks
Peak detection / settings
Peak integration
Peak statistics
Get peak statistics
Show monitor
Store peak shape for optimization/simulation
OK
Cancel

Fig. 2

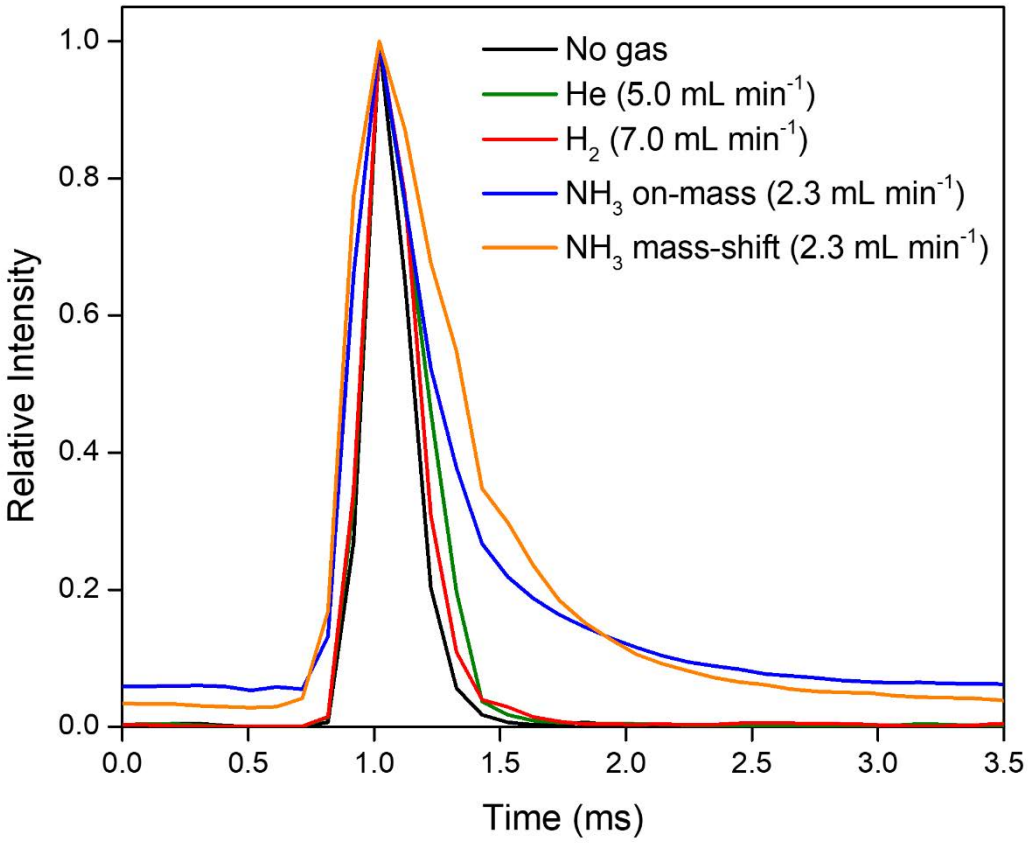
No gas
He (5.0 mL min-1)
H2 (7.0 mL min-1)
NH3 on-mass (2.3 mL min-1)
NH3 mass-shift (2.3 mL min-1)
Relative Intensity
Time (ms)
0.0
0.2
0.4
0.6
0.8
1.0
0.0
0.5
1.0
1.5
2.0
2.5
3.0
3.5

Fig. 3

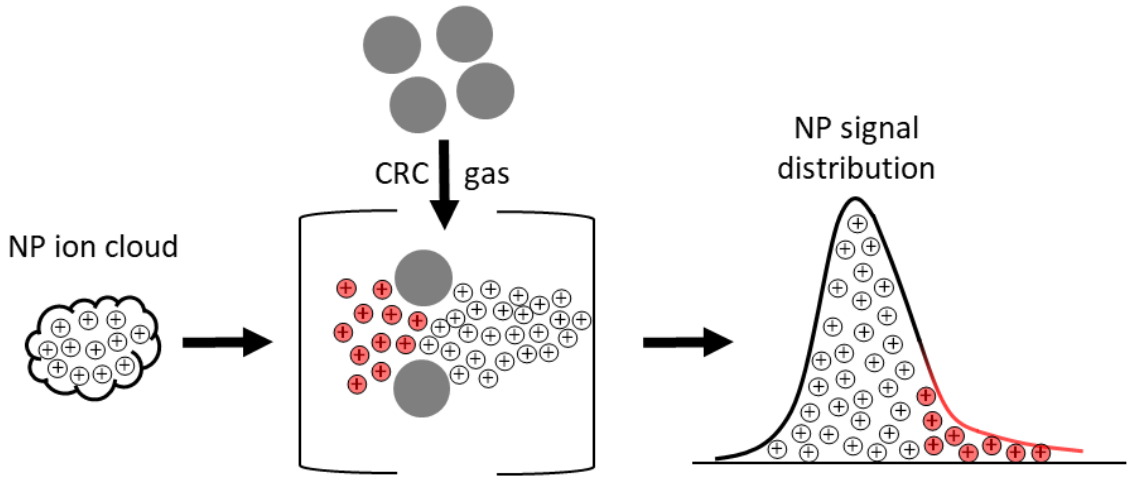

Fig. 4

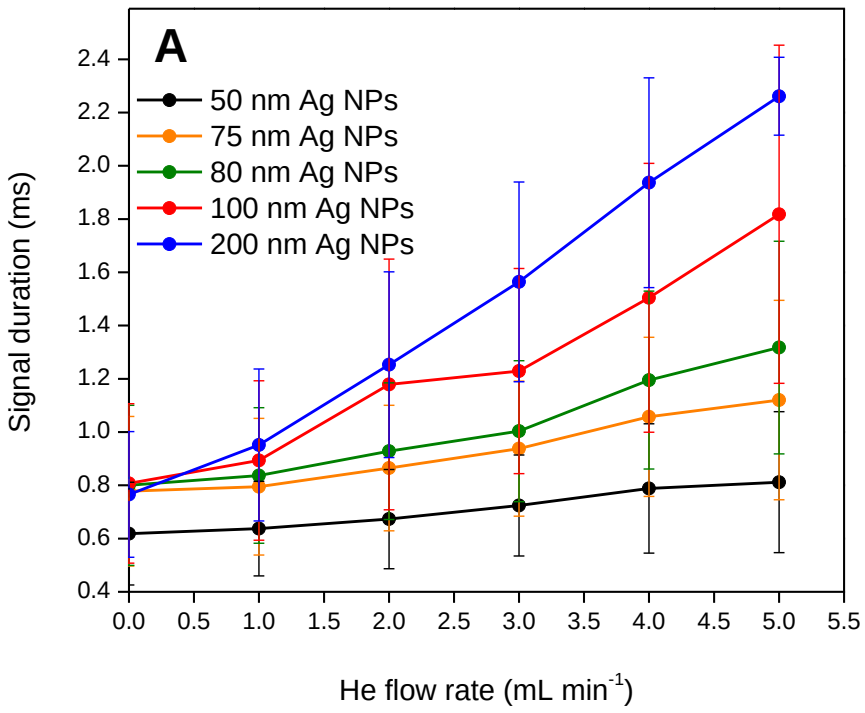
A
50 nm Ag NPs
75 nm Ag NPs
80 nm Ag NPs
100 nm Ag NPs
200 nm Ag NPs
Signal duration (ms)
He flow rate (mL min-1)

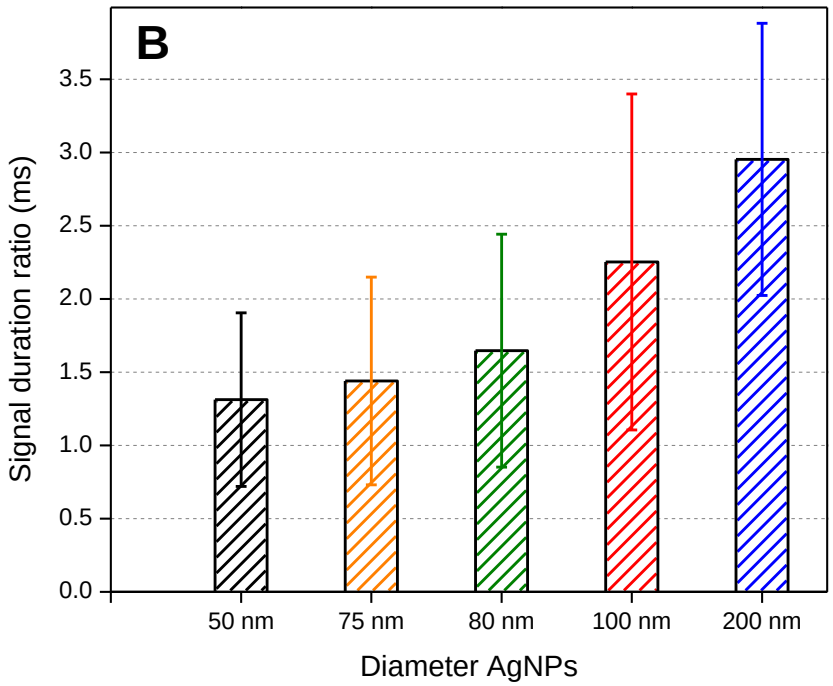
B
Signal duration ratio (ms)
50 nm
75 nm
80 nm
100 nm
200 nm
Diameter AgNPs

Fig. 5

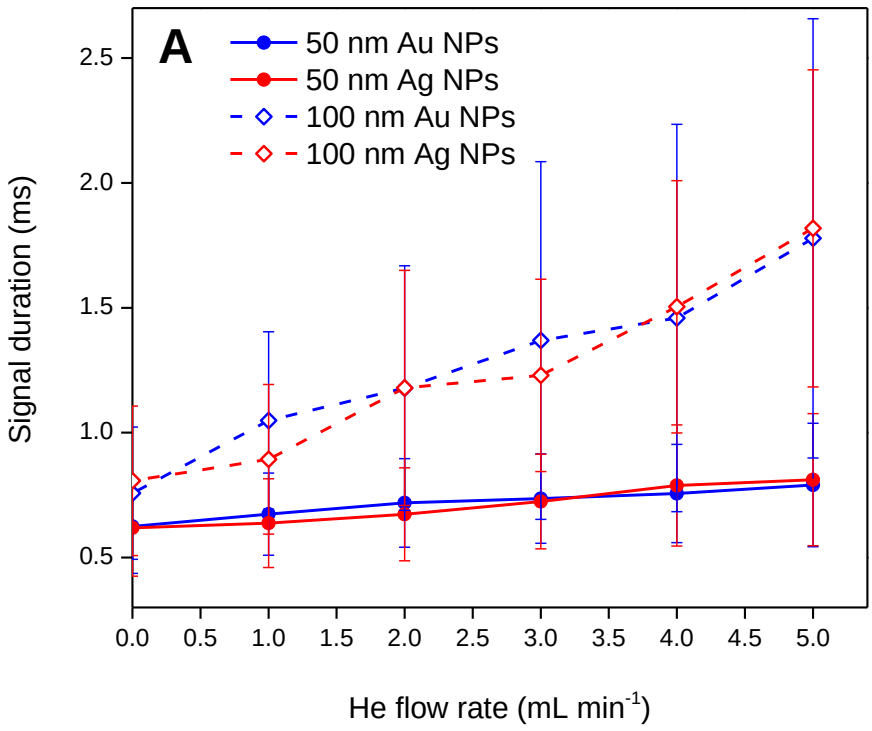
A
50 nm Au NPs
50 nm Ag NPs
100 nm Au NPs
100 nm Ag NPs
Signal duration (ms)
He flow rate (mL min-1)

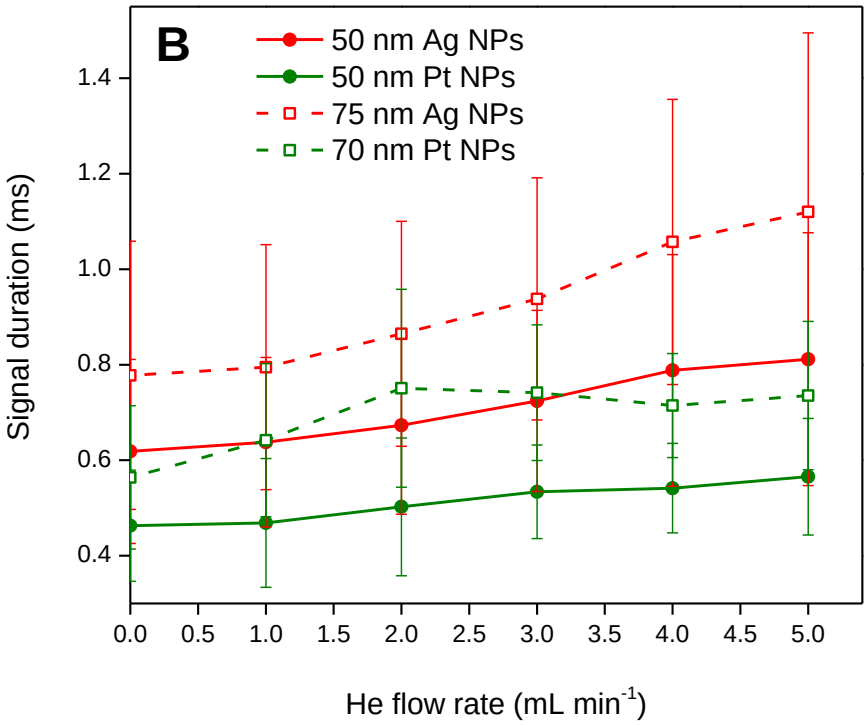
B
50 nm Ag NPs
50 nm Pt NPs
75 nm Ag NPs
70 nm Pt NPs
Signal duration (ms)
He flow rate (mL min-1)

Fig. 6

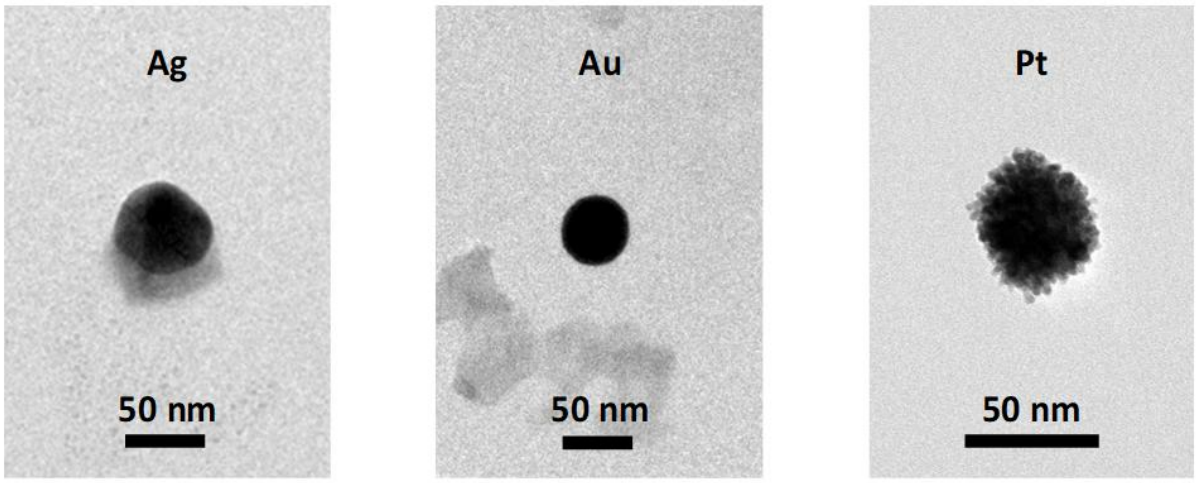

Fig. 7

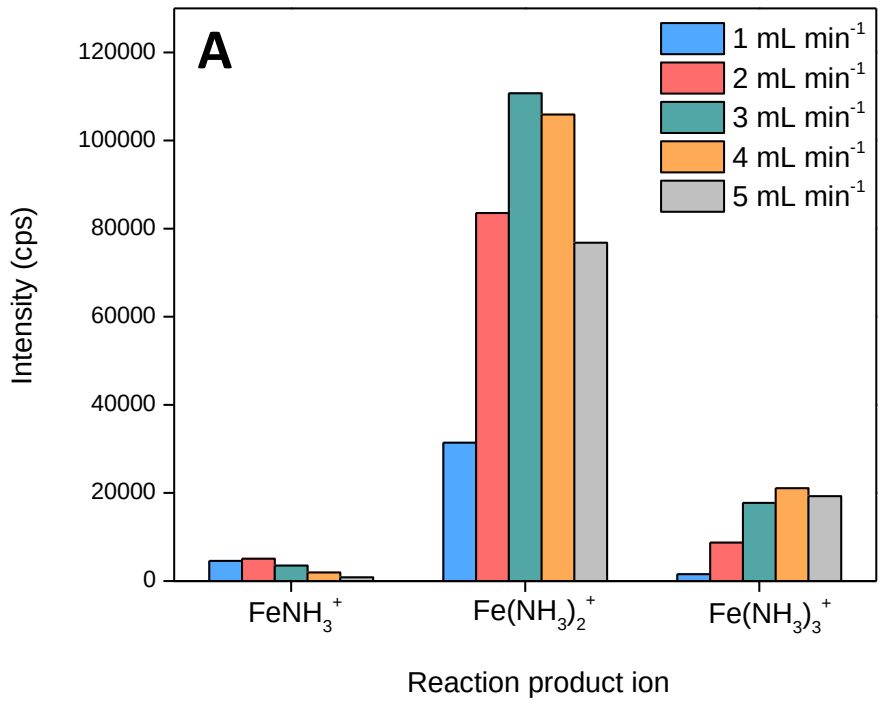
A
1 mL min-1
2 mL min-1
3 mL min-1
4 mL min-1
5 mL min-1
Intensity (cps)
120000
100000
80000
60000
40000
20000
0
FeNH3+
Fe(NH3)2+
Fe(NH3)3+
Reaction product ion

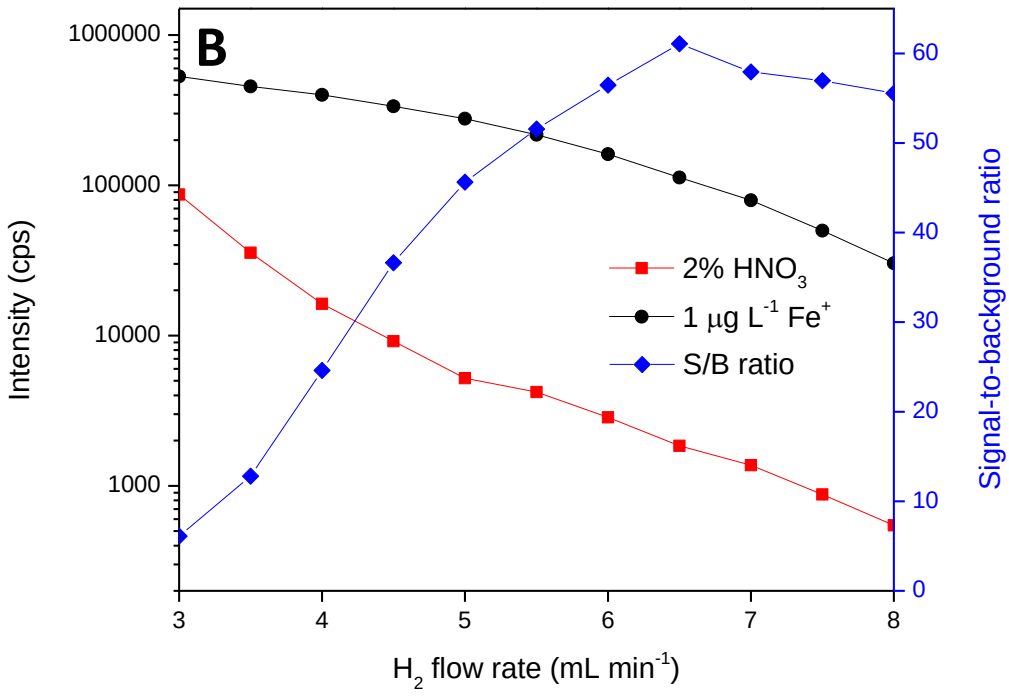
B
Intensity (cps)
1000000
100000
10000
1000
2% HNO3
1 μg L-1 Fe+
S/B ratio
Signal-to-background ratio
60
50
40
30
20
10
0
3
4
5
6
7
8
H2 flow rate (mL min-1)

Fig. 8

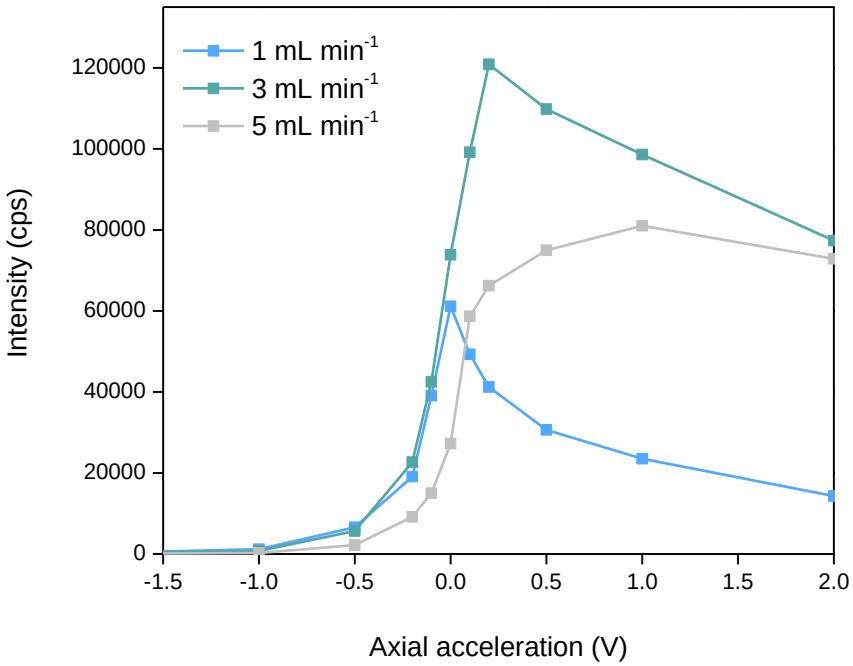
1 mL min-1
3 mL min-1
5 mL min-1
Intensity (cps)
120000
100000
80000
60000
40000
20000
0
-1.5
-1.0
-0.5
0.0
0.5
1.0
1.5
2.0
Axial acceleration (V)

Fig. 9

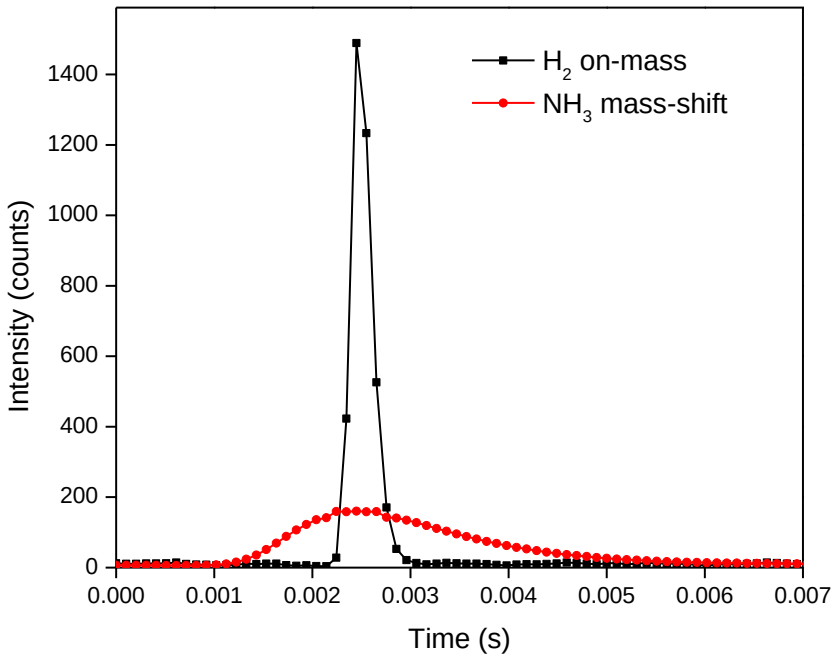
H2 on-mass
NH3 mass-shift
Intensity (counts)
Time (s)
0
200
400
600
800
1000
1200
1400
0.000
0.001
0.002
0.003
0.004
0.005
0.006
0.007

Fig. 10

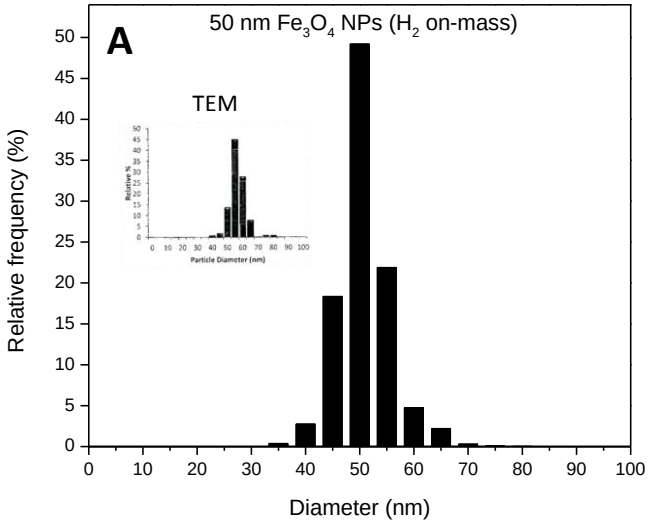
A
50 nm Fe3O4 NPs (H2 on-mass)
TEM
Relative frequency (%)
Diameter (nm)

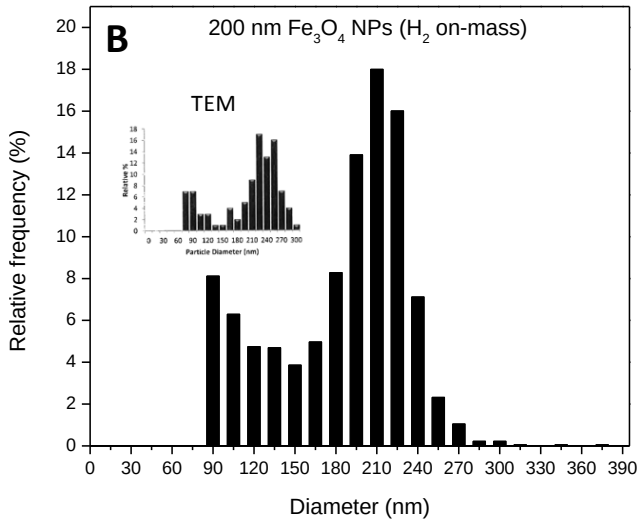
B
200 nm Fe3O4 NPs (H2 on-mass)
TEM
Relative frequency (%)
Diameter (nm)

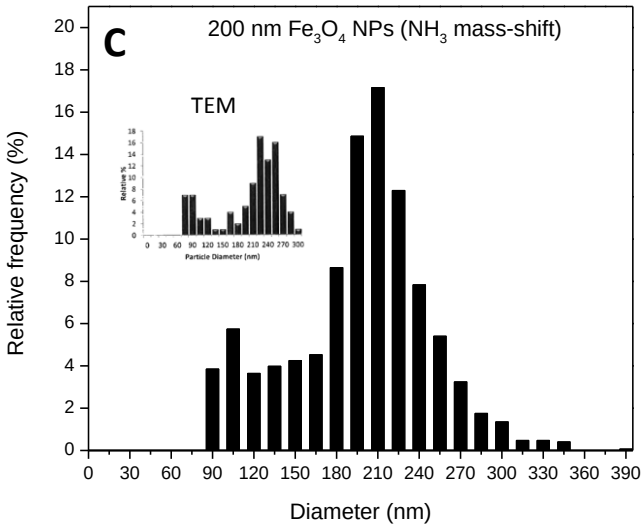
C
200 nm Fe3O4 NPs (NH3 mass-shift)
TEM
Relative frequency (%)
Diameter (nm)

Fig. 11

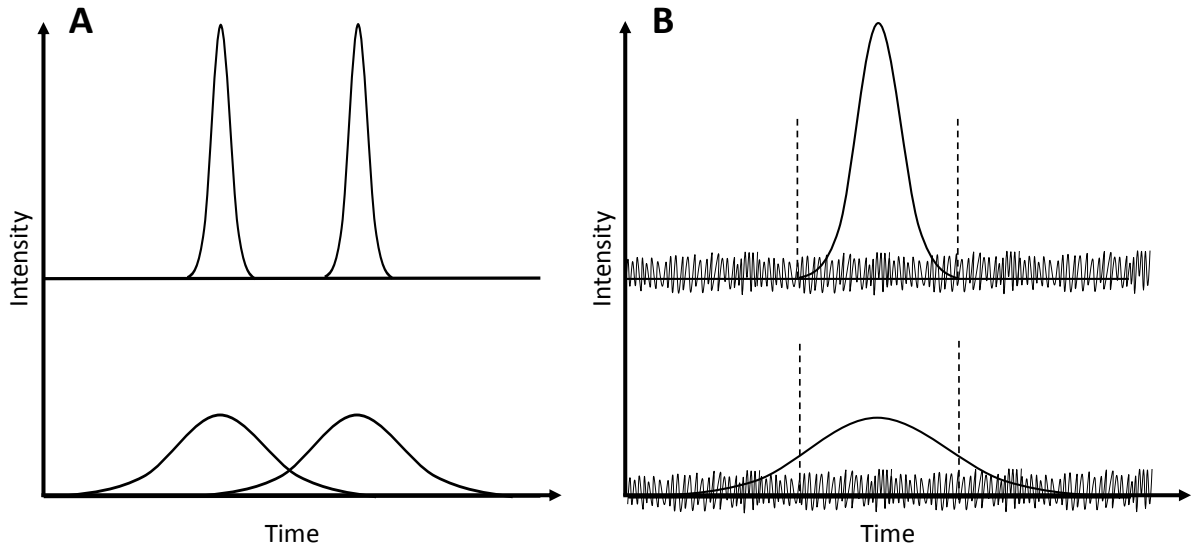

Table 1. Average peak width (signal duration) of individual NP events (signal spikes) at 1, 10 and 50% of the maximum height for the different CRC modes evaluated in this work.

		1% peak width	10% peak width	50% peak width
CRC mode	**Gas flow rate (mL min^{-1})**	**Average ± SD**	**Average ± SD**	**Average ± SD**
No gas	---	0.60 ± 0.10	0.40 ± 0.06	0.22 ± 0.03
No gas*	---	0.62 ± 0.13	0.41 ± 0.08	0.23 ± 0.04
H_2	7.0	0.63 ± 0.10	0.46 ± 0.09	0.24 ± 0.05
He	5.0	0.74 ± 0.13	0.46 ± 0.08	0.24 ± 0.04
NH_3 on-mass	2.3**	2.59 ± 0.91	1.33 ± 0.79	0.49 ± 0.32
NH_3 mass-shift*	2.3**	1.84 ± 0.86	1.22 ± 0.61	0.56 ± 0.13

*100 nm AuNPs were measured instead of 50 nm AuNPs.

**In the case of "NH_3", a mixture of 10% NH_3 in He was used. Additionally, 1 mL min^{-1} He was introduced automatically by the MassHunter software when the CRC is pressurized with NH_3/He.

Table 2. Probability of particle coincidence (P>1 – %) at different NP fluxes and peak widths calculated based on Poisson statistics.

	NP flux (Hz)		
Peak width (ms)	**5**	**20**	**50**
0.5	0.00031	0.0050	0.031
1.0	0.0012	0.020	0.12
2.5	0.0077	0.12	0.72
5.0	0.031	0.47	2.6